International Journal of Solids and Structures 196–197 (2020) 41–52

Contents lists available at ScienceDirect

International Journal of Solids and Structures

journal homepage: www.elsevier.com/locate/ijsolstr

How the spatial correlation in adhesion properties influences the performance of secondary bonding of laminated composites

Xiaole Li, Ran Tao, Arief Yudhanto, Gilles Lubineau*

King Abdullah University of Science and Technology (KAUST), Physical Sciences and Engineering Division (PSE), COHMAS Laboratory, Thuwal, 23955-6900, Saudi Arabia

A R T I C L E I N F O

Article history:
Received 8 March 2020
Revised 7 April 2020
Accepted 9 April 2020
Available online 22 April 2020

Keywords:
Secondary bonding
Delamination
Stochastic adhesion
Spatial correlation
Bridging

A B S T R A C T

Spatial heterogeneity of adhesion properties is known to result in bridging during debonding of secondary bonded composite joints. The ligaments that bridge both substrates have crack-arrest features and thus significantly enhance the fracture resistance of joints. We have investigated the effect of randomly distributed adhesion properties between the adhesive layer and each composite substrate in previous works; however, the spatial correlation of adhesion heterogeneity within or between the substrates and how it effects the failure of secondary bonded composites is still poorly understood. In this current work, we assume that the spatial heterogeneity of adhesion follows a log-normal distribution. The Napierian logarithm of interface toughness G_c and separating strength S can thus be described by a Gaussian Process. We investigate in detail the effect of spatial correlation both within each substrate and between opposite substrates. Finally, we predict the crack resistance of such joints with adhesives of different mechanical properties. We find that the failure strain of adhesives is important through varying the elongation of ligaments and thus the associated extra dissipated energy. This work represents the first critical step for designing tougher secondary bonded composite joints by triggering and controlling adhesive ligament bridging.

1. Introduction

Joining composites, such as fiber reinforced polymers (FRP), represents a design and manufacturing challenge. Adhesive secondary bonding has gained growing attention as a promising alternative to the traditional solutions that use fasteners or rivets to introduce mechanical interlocking (Budhe et al., 2017). A standard design of Adhesively Bonded Joints (ABJs) is of a sandwich type where two similar or dissimilar substrates (or adherends) are jointed by a thin adhesive (or adherent) layer. Various fracture modes may occur during debonding of ABJs, such as cohesive failure (within the adhesive), interfacial failure (at the adhesive/substrate interface) and, sometimes, hybrid fracture (a more complex combination of the two previous failure modes) (Tenchev and Falzon, 2007; Belnoue and Hallett, 2016; Tao et al., 2019). Hybrid failure is accompanied by the mechanisms of crack-tip transfer between alternating paths (Akisanya and Fleck, 1992). The associated ligament bridging the two paths (Tenchev and Falzon, 2007) is of interest because it can trap the propagation of the main crack and thus significantly enhance the fracture resistance of secondary bonded composites (Tao et al., 2019). Hybrid failure is closely related to a variety of properties including change in stress states (Cao and Evans, 1989; Akisanya, 2006; Saldanha et al., 2013) and heterogeneity in interfacial adhesion (Tao et al., 2019). Heterogeneity in adhesion refers to the spatially random distribution of interfacial bonding properties, which mainly results from the inherent morphology and the pre-treatment process of substrates (Moroni et al., 2018; Tao et al., 2018). The heterogeneous nature of surface morphology of composite substrates induces ubiquitous and unavoidable heterogeneous adhesion in the engineering of secondary bonded composites. In the context of FRP ABJs design, the effect of random distribution of adhesion properties on joints' performance should thus be emphasized.

This work is driven by two central motivations. First, a detailed evaluation of the random distributions of adhesion properties and their effects on FRP ABJs' debonding behaviors is essential for understanding the physical failure mechanisms that occur. This will provide more accurate numerical predictions of a joint's failure, which in turn can lead to the design of better performing structures. Second, an in-depth understanding into the mechanisms of toughening effects due to large-scale ligament bridging may lead to develop innovative FRP ABJs equipped with crack-arrest features

* Corresponding author.
E-mail addresses: xiaole.li@kaust.edu.sa (X. Li), gilles.lubineau@kaust.edu.sa (G. Lubineau).

https://doi.org/10.1016/j.ijsolstr.2020.04.012

through artificially enhancing and controlling the heterogeneity of adhesion.

The toughness enhancing mechanisms of crack-arrest/trap and bridging by tough particles (Mower and Argon, 1995; Bower and Ortiz, 1991) or fibers (Kaute et al., 1993; Sørensen and Jacobsen, 1998) in the case of two- or multiple-phase heterogeneous materials, *i.e.*, composites, have been extensively discussed (Tan et al., 2019; Kim et al., 2019; Mohamed et al., 2018; Sun et al., 2018; Naya et al., 2019). More generally, the strength and the fracture toughness of solids exhibiting heterogeneity in material properties have been discussed and the related stress dislocalization and crack-trap mechanisms have been investigated analytically and numerically (Dimas et al., 2016; 2015). The heterogeneity in adhesion may induce an analogical effect of crack-arrest produced by triggering ligament bridging. Conventional numerical approaches to model ABJs generally neglect the local complexity of failure by homogenizing a joint's bondline with a single cohesive zone (Srensen and Jacobsen, 1998; Da Silva and Campilho, 2012; Ivarez et al., 2014; Campilho et al., 2011). However, insights into the physical events undergoing locally during the debonding of ABJs, which cannot be provided by conventional approaches, are essential for obtaining a fundamental understanding of the mechanical behaviors of ABJs. Some efforts have been made towards clarifying the effects of flaws and randomness in bonding properties (Liner et al., 2019; Meng and Thouless, 2019; Taleb Ali et al., 2018; Ashcroft et al., 2012; Khokhar et al., 2009; Motamedi et al., 2014; Heide-Jrgensen and Budzik, 2018). The effect of the length scale of heterogeneity on bonding has also been discussed (Kammer et al., 2016; Dalmas et al., 2009; Chopin et al., 2015). Unfortunately, researches dedicated to excavating the local failure mechanisms of interest resulting from adhesion heterogeneity, *i.e.*, crack-tip transfer and ligament bridging, and the consequent arrest effects on the crack propagation of ABJs, are still very rare. Sills and Thouless (2015) considered strength discrepancy of interface in parallel cohesive zones and mimicked the phenomenon that the crack jumped from its original interface to the secondary interface with appropriate discrepancy subjected to a specific cohesive-length scale. They suggested that large-scale ligament bridging is a promising mechanism to be explored for toughening joints or materials. Botsis and coworkers Canal et al. (2016, 2017) developed a multi-scale based cohesive zone model in which the micromechanic fiber bridging in FRP laminates is characterized by a local heterogeneous embedded region (or core) to describe discrete arrangement of fibers. The authors' previous paper (Li et al., 2020) proposed a modeling strategy through two parallel cohesive zones with spatially stochastic interfacial properties to discriminate the failure within the sandwich configuration of ABJs. We applied this strategy to investigate the effect of variability in interfacial properties on the bonding performance of FRP ABJs (Li et al., 2020). The analysis of the quantitative data demonstrated that the spatially stochastic properties of adhesion significantly influence the debonding behaviors of FRP joints by triggering the mechanisms of crack-tip transfer and ligament bridging. The extrinsic dissipation contributed from the extra debonding surfaces and the plastic-damage of adhesives.

As mentioned above, adhesion shows randomness mainly due to the non-uniform morphology of adherend surfaces. A change in randomness/correlation of the heterogeneity may lead to various bonding behaviors of FRP ABJs. Regarding the modeling strategy that we proposed previously, the properties of adhesion at different locations along an interface between substrate and adhesives were regarded to be independent variables and were generated randomly based on specific probability distributions (in our case, log-normal distribution) without any spatial correlation. Thus, the joints spatially possessed discrete adhesion properties oscillating around the bonding baseline. A similar scheme to implement stochastic interfacial properties can be found in the work of Xu et al. (2014). Due to the non-uniformity attributed to multiple factors, *e.g.*, the spatial variations in the pretreatment quality, the interfacial properties should realistically distribute in a random but spatially correlated manner, rather than a non-correlated discrete variation as in the previous model. With uncorrelated stochastic interfacial properties, a numerical model may misestimate the occurrence of ligament bridging and the overall crack resistance of joints. A motivation of the present work is thus to improve the computational strategy by enabling a globally continuous and correlated variation of interfacial properties in space. We will then investigate the statistic effects of length scale in the spatial correlation of a stochastic interface and the correlation between two substrates on the structural response using the proposed model. We will vary the mechanical properties of adhesives and then predict the toughness of joints, to identify the important engineering parameters for toughening the FRP ABJs in the context of adhesion heterogeneity.

This work provides us with a better understanding of the stochastic bonding properties of FRP ABJs and points the way for designers to develop innovative FRP ABJs by artificially embedding adhesion heterogeneity and thus controlling the ligament bridging mechanisms.

2. A modeling strategy with stochastic interfacial properties using Gaussian process

2.1. The description of stochastic interfacial properties

We describe here how we introduce the spatial correlation in the adhesion properties of the adhesive/substrate interface.

As discussed in Li et al. (2020), a Gaussian process is suitable for describing the joint probability of the Napierian logarithm of the strength S and the toughness G_c of local adhesion. Dimas et al. employed Gaussian Process to conduct the modeling of an elastic solid with a heterogeneous Youngś modulus (Dimas et al., 2014), and demonstrated the toughening mechanisms resulting from crack-arrest and stress delocalization. In a Gaussian Process, any subset including points indexed by time or space of interests $\mathcal{X}$ is regarded to be a random vector $\mathbf{x} = [\mathbf{x}_1, \ldots, \mathbf{x}_\mathrm{n}] \in \mathcal{X}$ which follows a multivariate normal distribution. Suppose we have an n dimensional Gaussian distribution $\mathbf{x_1}, \ldots, \mathbf{x_n}$. The probability density distribution for multivariate Gaussian distribution is expressed as (Ahrendt, 2005):

$$f_{\mathbf{X}}(\mathbf{x}_1, \ldots, \mathbf{x}_n) = \frac{\exp\left(-\frac{1}{2}(\mathbf{x}-\boldsymbol{\mu})^{\mathrm{T}}\boldsymbol{\Sigma}^{-1}(\mathbf{x}-\boldsymbol{\mu})\right)}{\sqrt{(2\pi)^n|\boldsymbol{\Sigma}|}} \tag{1}$$

where $\boldsymbol{\mu}$ is the n-dimensional mean vector for the multivariate stochastic distribution. $|\boldsymbol{\Sigma}| \equiv \det \boldsymbol{\Sigma}$ is the determinant of the $n \times n$ symmetrix covariance matrix $\boldsymbol{\Sigma}$.

The schematic on Fig. 1 represents a general interface whose properties follow a Gaussian Process. The dots stand for the integration points of cohesive elements as a subset indexed by their spatial coordinates. In this Gaussian Process, the subset composed by the dots is the spatial supporter to draw samples of n-dimensional multivariable Gaussian distribution. Following Li et al. (2020), in the context of adhesion, this Gaussian process holds for the Napierian logarithm of the strength S and the toughness G_c. We then have for the properties along the interface at any coordinate $\mathbf{x}_i$:

$$(\ln(S)_i, \ln(G_c)_i) \sim \mathcal{N}\left(\rho, \mu_{\ln(S)}, \sigma_{\ln(S)}, \mu_{\ln(G_c)}, \sigma_{\ln(G_c)}\right) \tag{2}$$

in which ρ is the Pearson product-moment correlation coefficient of $\ln(S)$ and $\ln(G_c)$, $\mu_{\ln(S)}$ and $\sigma_{\ln(S)}$ are the mean and variance of $\ln(S)$ respectively, $\mu_{\ln(S)}$ and $\sigma_{\ln(G_c)}$ the mean and variance of $\ln(G_c)$, respectively. We recall that the mean and variance of logarithm of any variable a following log-normal distribution can be

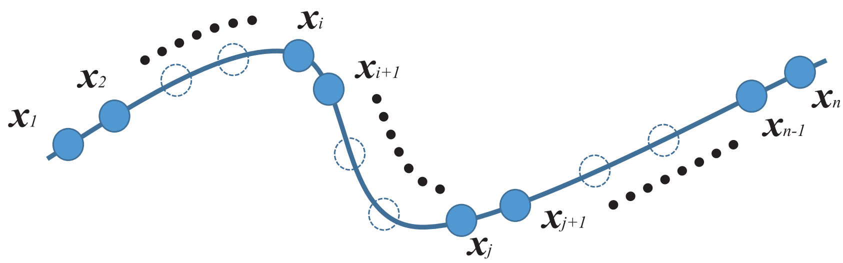

Fig. 1. Schematic of an interface with stochastic properties described by Gaussian Process.

calculated by:

$$\mu_{\ln(a)} = \ln\left(\frac{\mu_a}{\sqrt{1+\frac{\sigma_a^2}{\mu_a^2}}}\right), \quad \sigma_{\ln(a)}^2 = \ln\left(1+\frac{\sigma_a^2}{\mu_a^2}\right) \tag{3}$$

Under a finite number of sampling spatial points as shown in Fig. 1, the corresponding adhesion properties for the sample along the interface following Gaussian Process have distribution:

$$\begin{bmatrix} \ln(\mathbf{S}) \\ \ln(\mathbf{G}_c) \end{bmatrix} \sim \mathcal{N}\left(\begin{bmatrix} \boldsymbol{\mu}_{\ln(\mathbf{S})} \\ \boldsymbol{\mu}_{\ln(\mathbf{G}_c)} \end{bmatrix}, \begin{bmatrix} \Sigma\left(\mathbf{x}_{\ln(\mathbf{S})}, \mathbf{x}'_{\ln(\mathbf{S})}\right) & \Sigma\left(\mathbf{x}_{\ln(\mathbf{S})}, \mathbf{x}'_{\ln(\mathbf{G}_c)}\right) \\ \Sigma\left(\mathbf{x}_{\ln(\mathbf{G}_c)}, \mathbf{x}'_{\ln(\mathbf{S})}\right) & \Sigma\left(\mathbf{x}_{\ln(\mathbf{G}_c)}, \mathbf{x}'_{\ln(\mathbf{G}_c)}\right) \end{bmatrix}\right) \tag{4}$$

in which

$$\begin{aligned} \mathbf{S} &= [S(\mathbf{x}_1), \ldots, S(\mathbf{x}_n)]^T \\ \mathbf{G}_c &= [G_c(\mathbf{x}_1), \ldots, G_c(\mathbf{x}_n)]^T \end{aligned} \tag{5}$$

and

$$\begin{aligned} \boldsymbol{\mu}_{\ln(S)} &= \left[\mu_{\ln(S)}(\mathbf{x}_1), \ldots, \mu_{\ln(S)}(\mathbf{x}_n)\right]^T \\ \boldsymbol{\mu}_{\ln(G_c)} &= \left[\mu_{\ln(G_c)}(\mathbf{x}_1), \ldots, \mu_{\ln(G_c)}(\mathbf{x}_n)\right]^T \end{aligned} \tag{6}$$

The sub-matrices of the covariance matrix are defined as:

$$\begin{aligned} &\Sigma\left(\mathbf{x}_{\ln(\mathbf{S})}, \mathbf{x}'_{\ln(\mathbf{S})}\right) = \sigma_{\ln(\mathbf{S})}^2 K \\ &\Sigma\left(\mathbf{x}_{\ln(\mathbf{G}_c)}, \mathbf{x}'_{\ln(\mathbf{G}_c)}\right) = \sigma_{\ln(\mathbf{G}_c)}^2 K \\ &\Sigma\left(\mathbf{x}_{\ln(\mathbf{S})}, \mathbf{x}'_{\ln(\mathbf{G}_c)}\right) = \Sigma\left(\mathbf{x}_{\ln(\mathbf{G}_c)}, \mathbf{x}'_{\ln(\mathbf{S})}\right) = \rho\sigma_{\ln(\mathbf{S})}\sigma_{\ln(\mathbf{G}_c)} K \end{aligned} \tag{7}$$

in which the matrix K is the kernel matrix which is generated *via* a kernel function k, a characteristic of the Gaussian Process:

$$K = \begin{bmatrix} k(\mathbf{x}_1, \mathbf{x}_1) & \cdots & k(\mathbf{x}_1, \mathbf{x}_n) \\ \vdots & \ddots & \vdots \\ k(\mathbf{x}_n, \mathbf{x}_1) & \cdots & k(\mathbf{x}_n, \mathbf{x}_n) \end{bmatrix} \tag{8}$$

The widely used exponential kernel is deployed here as it has the potential to adequately describe correlations in properties due to correlation in geometrical features such as roughness:

$$k\left(\mathbf{x}_i, \mathbf{x}_j\right) = \exp\left\{-\left(\frac{\left|\mathbf{x}_i - \mathbf{x}_j\right|}{r}\right)^{\alpha}\right\} \tag{9}$$

Using $\alpha = 1$, $r = 0.5$ and $x_2 = 8$, the exponential kernel $k(x_1, x_2)$ is visualized in Fig. 2, which equals 1 when $x_1 = x_2$ (highest co-variance) and tends to be 0 as its arguments drift apart (uncorrelated).

Because for a general secondary bonded joint, the morphology and the pre-treatment for the surfaces of the two facing substrates are a priori not related, we assume that the two interfaces of the bondline follow two uncorrelated Gaussian Processes, but with similar characteristic parameters, as processing is usually performed in the same way on both surfaces.

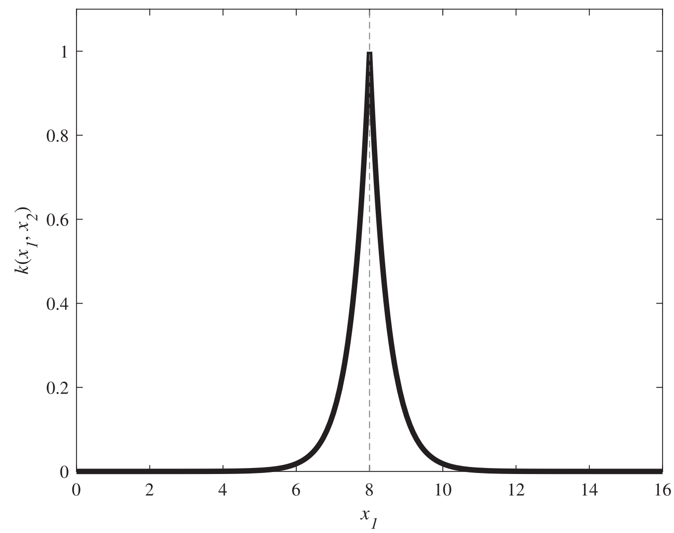

Fig. 2. Visualization of the exponential kernel $k(x_1, 8)$ in the range of $x_1 \in (0, 16)$.

2.2. The finite element (FE) model and Monte Carlo simulation

We used the same FE model of the FRP Double Cantilever Beam (DCB) as in Li et al. (2020). The configuration and boundary conditions of the DCB are shown in Fig. 3. Each substrate is unidirectional with a thickness of 2 mm. The bondline thickness is fixed as 0.15 mm. The two interfaces, with nearly zero thickness, follow two independent Gaussian Processes.

Concerning the substrates, the material was modeled as linear elastic orthotropic and the material of the adhesive was modeled as coupled elasto-plastic with damage. The properties are summarized in Tables 1 and 2.

Concerning the modeling of the interfaces, we first need to elucidate the correlation between S and G_c. To do so, we carried out experiments of single lap joints subjected to three points bending whose failure is governed by S, and DCB whose failure is governed by G_c. Two groups of specimen, the substrates of which were pretreated by laser with two different pulse fluences to access different morphologies, named as L1 and L2, were tested. S could obviously not be measured directly but was numerically estimated by calibrating simulations of the single lap joints with respect to the experimental results. Fig. 4 shows the results, which clearly indicate a negative correlation between S and G_c. Therefore, the correlation coefficient ρ was kept to be −1 when generating the heterogeneous adhesion. The expected values of S and G_c were set as the average of those of the ABJs pretreated with L1 and L2, which were $\mu_S = 21.5$ Mpa and $\mu_{G_c} = 0.24$ KJ/m^2 with a standard deviation of 2.5 and 0.04, respectively. The effects of deviation and correlation coefficient ρ on macroscopic crack resistance of ABJs were clarified in the last paper (Li et al., 2020).

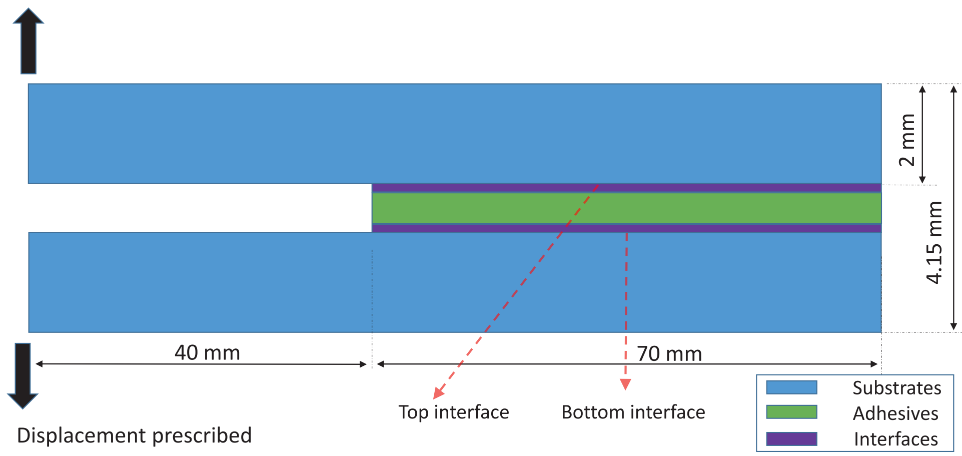

Fig. 3. The configuration and boundary conditions of the modeled DCB. (For interpretation of the references to color in this figure legend, the reader is referred to the web version of this article.)

Table 1
The material properties of the elastic substrates.

Carbon/Epoxy lamina (M21/T700)				
E_{11} (MPa)	E_{22} (MPa)	E_{33} (MPa)	$\nu_{12} = \nu_{13} = \nu_{23}$	$G_{12} = G_{13} = G_{23}$ (MPa)
125000	7800	7800	0.33	5100

Table 2
The materials properties of adhesives used in numerical model.

Epoxy adhesive (Araldite®420) (Haider et al., 2011; De Moura et al., 2006)					
E (MPa)	ν	σ_e (MPa)	σ_u (Mpa)	ϵ_u	G_f (KJ/m^2)
1500	0.33	27	37	3.4%	0.022

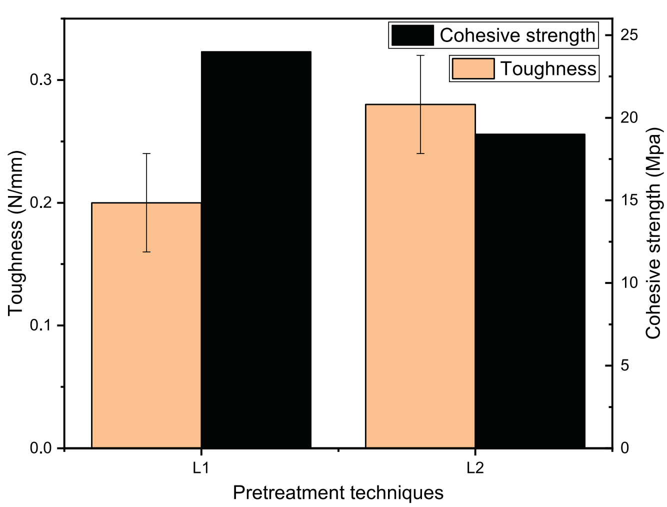

Fig. 4. The experimentally measured S and G_c of composite joints whose substrates were pre-treated by laser ablations with different laser fluences, L1 and L2. (For interpretation of the references to color in this figure legend, the reader is referred to the web version of this article.).

Considering the success to model the plasticity of epoxy (Yang et al., 2004; Cooper et al., 2012) and ease to use, the classical **J2** flow theory of plasticity with linear isotropic hardening (de Souza Neto et al., 2011) was employed to characterize the elastoplastic constitutive behavior of epoxy adhesives. In the implementation, backward Euler algorithm is employed to complete the time integration of the plastic strain for each pseudo time increment. The ductile criterion (Hillerborg et al., 1976) was used to predict the onset of damage in adhesives. The equivalent plastic strain at the onset of damage is normally a function of stress triaxiality and strain rate. To simplify the question, herein the damage of adhesives was assumed to be rate independent and triaxiality independent. We assumed the effective response of the adhesive is perfectly plastic beyond the onset of damage, and we employed the linear damage evolution equation to characterize the softening process. Then, the state variable to describe material degradation increases monotonically and linearly with plastic deformation.

To achieve reliable statistical analysis, we conducted Monte Carlo simulation. A set of characteristic parameters of the stochastic heterogeneity can be applied to generate extensive groups of realizations of parallel interfaces, each of which is used to model a sample of ABJs subjected to the corresponding stochastic properties. Predictions of all the samples constitute a Monte Carlo simulation of the set. The FE models were run with ABAQUS V6.17 on a workstation with 16 Intel Xeon(R) W-2145 CPUs @ 3.7 GHz. Fig. 5 presents the evolution of the mean number of the formed ligaments and the mean toughness (macroscopic toughness) with the increase of sample number (50 samples were drawn and run for the Monte Carlo simulation). The correlation length r was set at 5 mm in this Monte Carlo simulation. It is clear that after 30 runs in this Monte Carlo simulation, predictions were reasonably achieving statistical convergence. To achieve a reliable prediction with relatively low computational burden, we ran 50 samples for each Monte Carlo analysis of correlation length in the following investigation.

3. Effect of correlation characteristics on the macroscopic joint performance

3.1. Effect of correlation within substrates

We first study the effect of having spatial correlation in adhesion properties within each substrate. Such correlation can be a natural consequence of the pretreatment technique that usually introduces a length-scale and thus a correlated morphology. However, no correlation is assumed at this stage between the two opposite substrates of the joint. Fig. 6 shows the typical spatial dis-

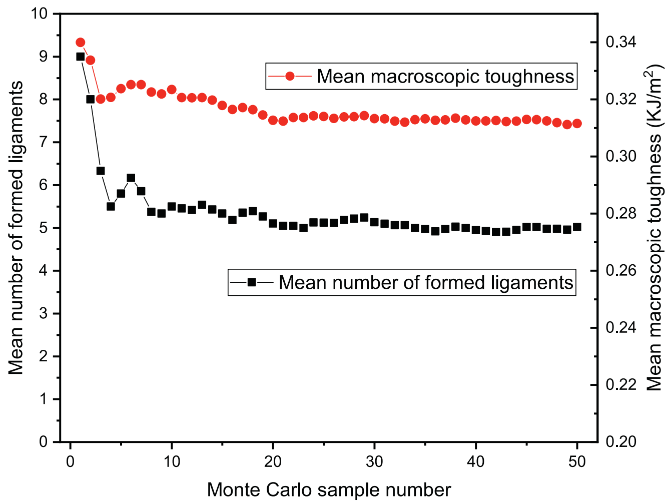

Fig. 5. The variation of the statistical results with the increase sampling of Monte Carlo simulation.

tributions of S along the two parallel interfaces subjected to the different length scales of correlation that we evaluated. The pattern of the distribution in Fig. 6 is similar with the surface profiles of composite substrates measured by Tao et al. (2018), which somehow confirms the applicability of the exponential kernel to describe the spatial correlation of adhesion heterogeneity. It can be seen from Fig. 6 that with the increase of r, the wave length of the fluctuation tends to increase. Physically, a larger correlation length means that the morphology of the surface is changing smoothly in space.

Fig. 7 presents the statistical outcomes of the macroscopic toughness and the number of ligaments formed during debonding of the joints subjected to different spatial correlations corresponding to the length scales shown in Fig. 6. Compliance calibration (Berry, 1963) was used to perform the data reduction. The propagation of crack advances from $\Delta a = 0$ mm to $\Delta a = 55$ mm was considered when calculating the macroscopic toughness. A clear positive relationship between the number of ligaments and the macroscopic toughness is indicated. Under relatively low spatial correlation (with smaller r), the random heterogeneity of interfacial adhesion can significantly promote the occurrence of crack-tip transfer, adding more crack-arrest features, in terms of large-scale ligament bridging, into the system and enabling the joint to be tougher.

Moroni et al. (2018) showed that the joints, whose substrates were pre-treated with the same technique (laser ablation) with different treatment parameters, *i.e.*, laser energy density, produced diverse failure modes and demonstrated different toughness. Our study provides possible explanation for these observations. Indeed, different laser treatments can result in different surface morphologies and correlation in adhesion properties. Our simulations show an overall increasing trend with the decrease of r. Only the prediction of the joints subjected to $r \to 0$ mm is lower than that from the joints subjected to $r = 0.5$ mm, which is with the most significant enhancement in macroscopic toughness exceeding the baseline value by about 54.6%.

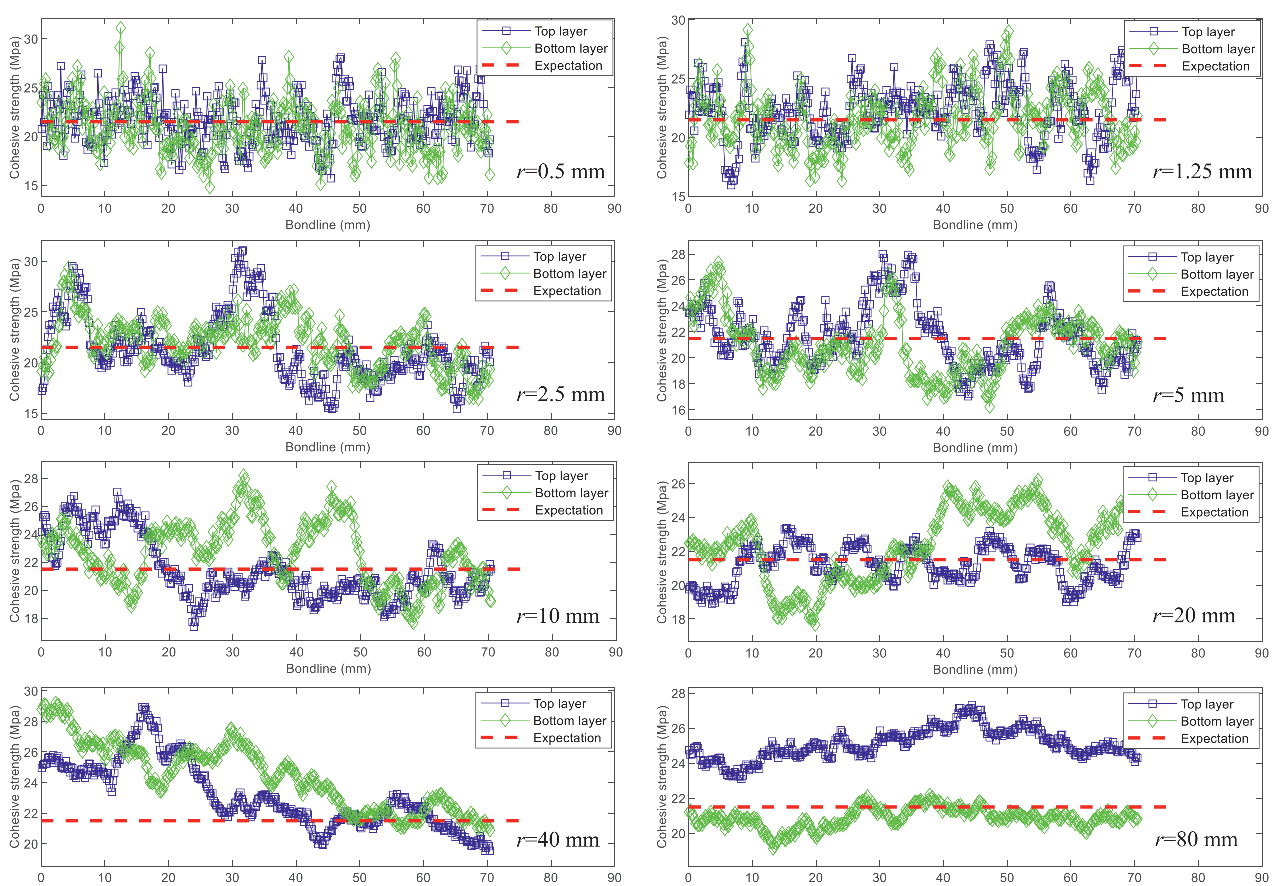

Fig. 6. The spatial distributions of interfacial strength S realized through the proposed algorithm subjected to different spatial correlation length r.

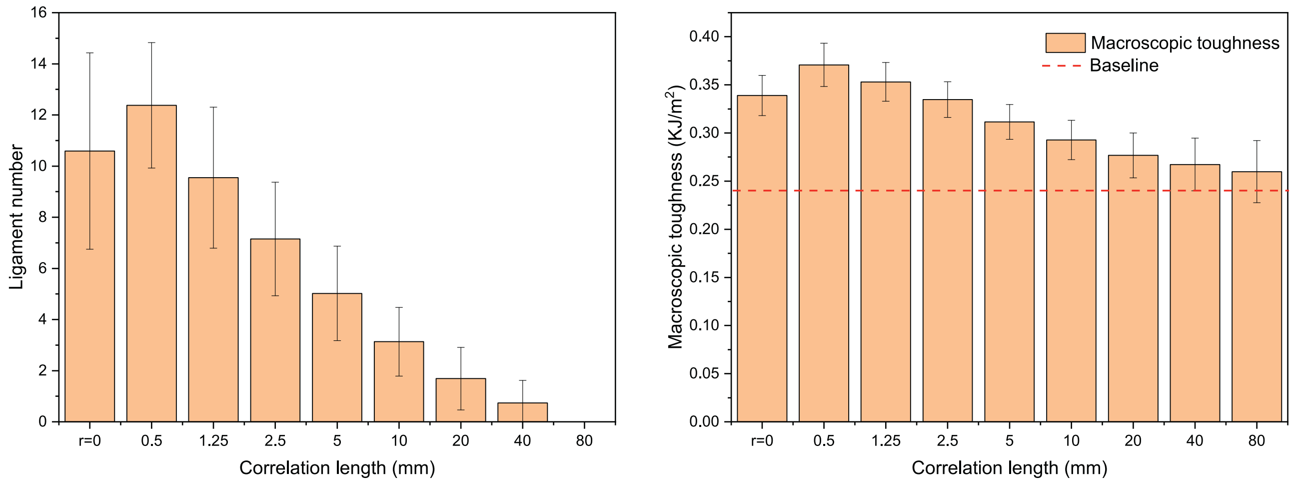

(a) ligament number *vs.* correlation length r

(b) macroscopic toughness *vs.* correlation length r

Fig. 7. The effects of the spatial correlation length of the adhesion's heterogeneity on the debonding performance of ABJs.

In what follows, we analyze two limiting cases. Theoretically, infinitesimal r results in globally homogeneous adhesion. We expect the system to behave homogeneously and demonstrate identical performance with the baseline joint. However, the discrete nature of the finite element model, depending on mesh size, induces a lower limit to the effective r that the model can characterize, and thus the case of $r \to 0$ in the present study is not physically infinitesimal. The corresponding joints are still with adhesion heterogeneity and thus establish considerable ligament bridging (see Fig. 7a) but with a reduction of the effectiveness of crack trapping by about 9.7% compared to the $r = 0.5$ mm case. Consequently, an upper bound of the toughness of ABJs was erected with decreasing r (see the case of $r = 0.5$ for example), which explains why the macroscopic toughness of the joints subjected to $r \to 0$, obtained from Monte Carlo simulation, is smaller than that of the joints subjected to $r = 0.5$ mm but higher than the baseline. Based on the observations from Fig. 7, we can reasonably suppose that the toughness of joints may achieve a maximum with an appropriate correlation length of the adhesion's heterogeneity. This critical length may depend on multiple factors, such as heterogeneity characteristics and bondline thickness.

Provided the correlation length becomes very large in the limit, the parallel interfaces constituting the bondline of finite length then have nearly uniform but random properties. No ligament will be formed for such joints and thus the macroscopic toughness will be contributed from pure interfacial fracture, as revealed by the joint subjected to $r = 80$ mm. Notably, the observed toughness in the case of $r = 80$ mm is higher than the expected value (baseline) of interface properties, which is counterintuitive. This is because S is a more important parameter for crack nucleation and crack-tip transfer. In the scenario of pure interfacial failure, crack tends to nucleate and propagate at the interface with lower S. Under negative correlation between S and G_c, the interface with low S always possesses higher G_c compared to the parallel interface. The macroscopic toughness should be the average toughness of the debonded interface. Statistically, this value tends to be higher than the baseline. A theoretical interpretation can be found in Appendix A. The above analysis regarding the two limiting cases is consistent with the discussions in the work of Dimas et al. (2014) focusing on the influence of heterogeneity of Young's modulus and strength on general solids. The reality is somewhere between these two ideal cases.

3.2. Effect of correlation between substrates

The ability of correlation in adhesion properties to largely modified the toughening effect resulting from bridging paves the way for new design strategies in which the correlation between substrates is artificially controlled to optimize the bridging effect. The protocol of design can be a bondline with periodical fluctuation, *e.g.* trigonometric waviness, in adhesion properties. The anticipated crack resistance may benefit from the periodically occurred ligament bridging mechanisms.

As a first step, we explore the effect of the correlation of the properties between the opposite substrates. In the case of trigonometric waviness, the phase difference of alignment, $\Delta\phi$, is the main parameter that characterizes the correlation between the two substrates. Herein, the period of the fluctuation was 4 mm. To ensure the practical feasibility of the protocol, we used the measured bonding properties of $L1$ and $L2$ as the upper and lower bounds of the properties, and the amplitude of fluctuation is thus the difference between them. In the simulations, we varied $\Delta\phi$ from 0 to π. The generated fluctuated adhesion (only the fluctuation within two periods is present) is as shown in Fig. 8, where negative correlation between S and G_c was kept. In engineering practice, we can achieve the fluctuating adhesion by smoothly changing the pulse fluence of laser ablation with the moving of laser beam.

Fig. 9 presents the predicted load P *vs.* crack opening δ curves and R-curves. The presence of the fluctuation in adhesion within the process zone is manifested by the undulations in the $P - \delta$ responses as well as the R-curve behaviors of joints.

In the cases of $\Delta\phi = 0$, 0.125π and 0.25π, no crack-tip transfer occurred. For such joints, the undulations in the $P - \delta$ responses and the R-curve behaviors are purely attributed to the fluctuated interface properties. Thus, at the macroscopic level, the R-curve behaviors are similar (but not perfectly matching) to the input, *i.e.*, the sinusoidal waviness of toughness. The theoretical interpretation of why the R-curve behaviors are not in an excellent match with the input is presented in Appendix B.

With the increase of $\Delta\phi$, the maximum discrepancy of adhesion properties at the corresponding coordinates between the parallel cohesive zones is also increasing, as indicated by the curve in Fig. 10a. To alternate the crack path, the maximum discrepancy of adhesion properties must reach the critical condition. In these cases, the joints experience a process of establishing a stable R-curve behavior. Initially, the toughness of joints equals the

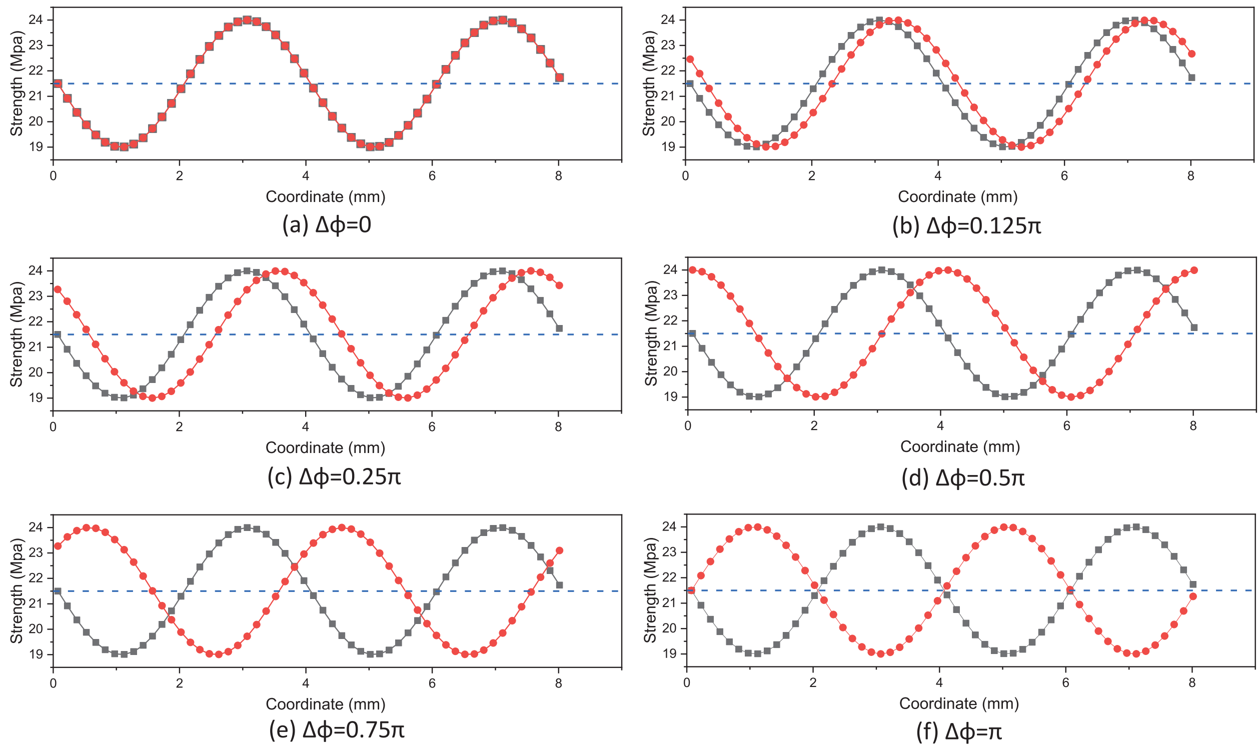

Fig. 8. The generated interfacial strength S with fluctuations subjected to different phase difference $\Delta\phi$ of alignment. The round dot signifies the top interface and the square dot the bottom interface.

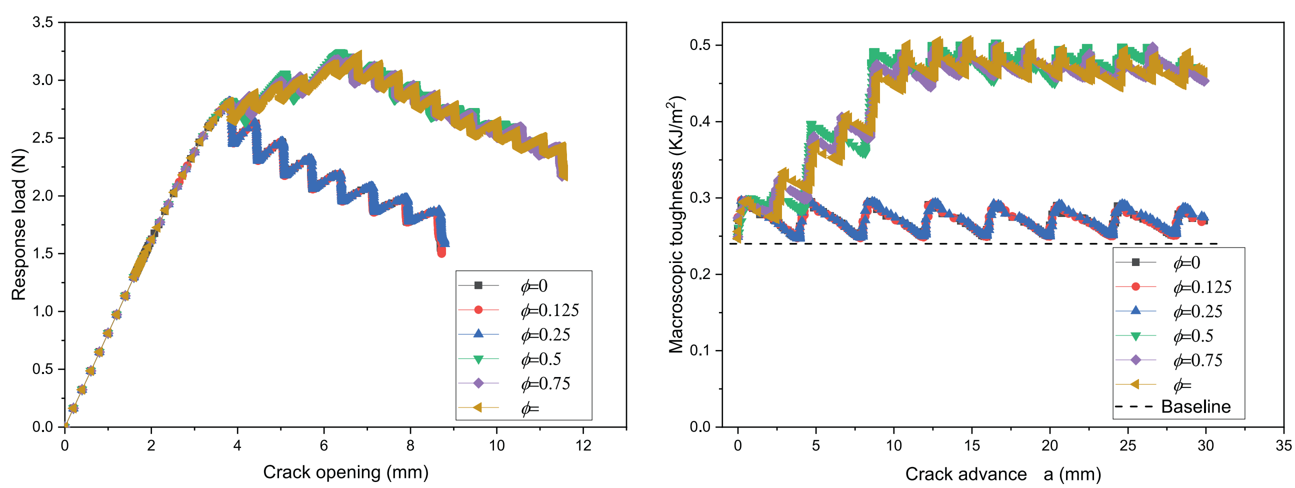

(a) P-δ curves (b) R-curves

Fig. 9. The $P-\delta$ curves and the R-curves obtained from the ABJs with fluctuated adhesion.

interfacial toughness of the weaker adhesion, but it gradually increases with increasing crack lengths before the full establishment of large-scale ligament bridging at around $\Delta a = 8$ mm. Afterwards, its progression is hindered by crack-arrest mechanisms whose period is the same with that of the input fluctuation. The R-curves keep oscillating around a plateau value that is about 93% higher than the baseline value and are insensitive to the change in the alignment phase of the adhesion fluctuation. The overall trend of R-curve behaviors obtained from such joints is quite similar to the observations in delamination of FRP laminate with fiber bridging (Pappas and Botsis, 2020). Once $\Delta\phi$ is qualified to periodically trigger the crack-tip transfer and the subsequent bridging, there is no significant difference in the effectiveness of crack-arrest. This conclusion favors the application of the proposed protocol, because it will facilitate the operation of joining. There is no need to strictly match the adherend surfaces to find the optimum alignment phase as long as it is guaranteed that $\Delta\phi$ between the substrates is within the range that the crack-tip transfer can be triggered.

We also performed simulations for the FRP ABJs with adhesives thickness of $t = 0.12$ and $t = 0.18$ mm to verify the bondline thickness effect. As shown in Fig. 10a, for all $\Delta\phi$ under consideration, the minimum $\Delta\phi$ qualified to trigger bridging increases with increasing bondline thickness. The minimum qualified discrepancy of adhesion properties changes with an increase in t, which is the es-

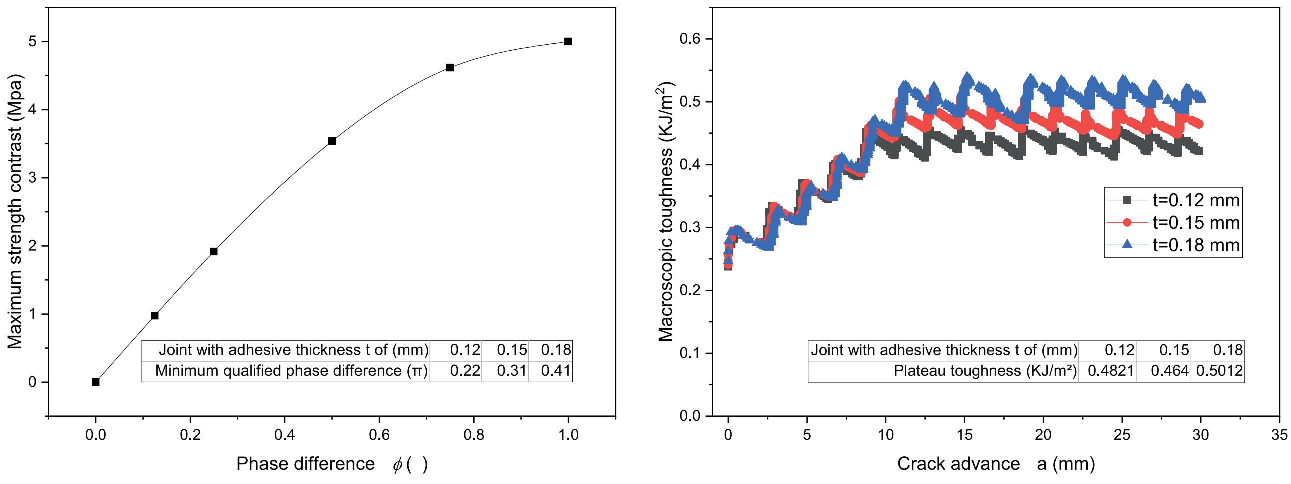

(a) (b)

Fig. 10. (a) The curve of maximum contrast of S with the change of $\Delta\phi$, and the minimum $\Delta\phi$ qualified to trigger ligament bridging for different bondline thicknesses, listed in the table on the bottom of figure; (b) The comparison of R-curve behaviors of the ABJs with adhesive of different bondline thicknesses, and the plateau values listed in the table on the bottom of figure. ($\Delta\phi = \pi$).

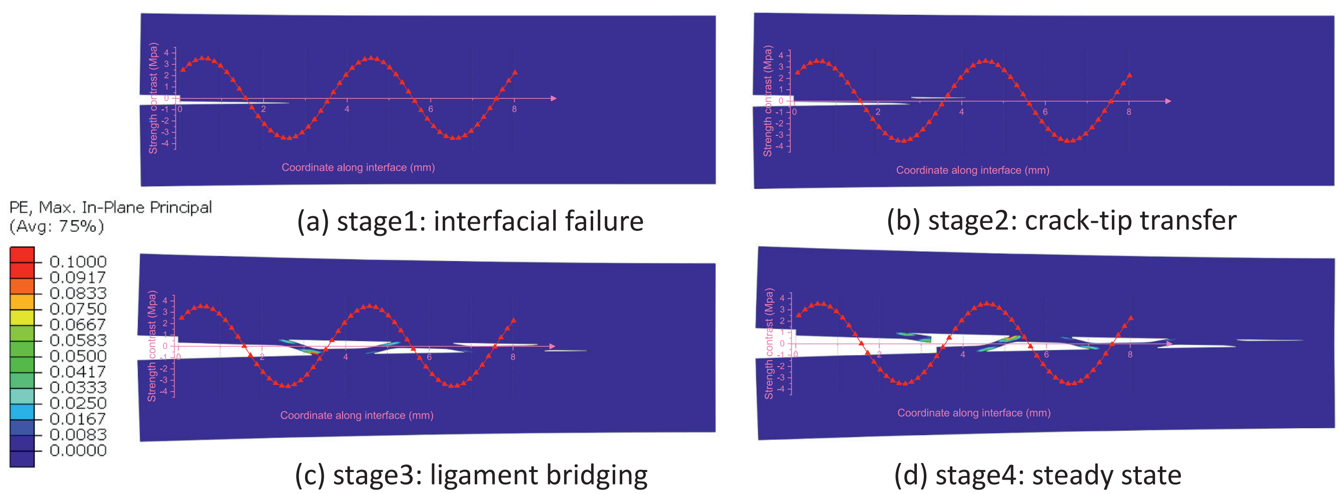

Fig. 11. Typical debonding process of a joint with the adhesion of fluctuated heterogeneity (The variation of the strength contrasts along the interfaces is superimposed).

sential origin of the bondline thickness effect. From the R-curve behaviors shown in Fig. 10b, the plateau value of R-curve (macroscopic toughness) exhibits an increasing trend with the increasing bondline thickness. Therefore, under the condition that ligament bridging can be triggered, a thicker adhesive layer may provide more significant enhancement in macroscopic toughness.

Fig. 11 presents a complete establishment of large-scale bridging in a joint with the presence of the adhesion heterogeneity qualified to trigger crack-tip transfer ($\Delta\phi = 0.5\pi$). The strength contrast between the parallel interfaces ($S_{top} - S_{bottom}$) as a function of the spatial coordinate along the interface is superimposed on the segment of crack propagation. We can see that in stage 1, the debonding is a pure interfacial fracture, and then the crack advance stops in its original interface and a new crack nucleates in the secondary interface in stage 2. The location of the crack-tip transfer is around the turning points where the maximum contrasts of the adhesion properties of the top interface and bottom interface are. Thus, the crack-tip transfer altering crack path occurs, subsequently, in stage 3 the adhesive ligament behaves as a beam to bridge the adherends and suppresses the crack, and the so-called crack-arrest features take effect on the overall behavior of the joint. Multiple ligaments have been formed in the same timeframe as shown in Fig. 11(c), approaching a steady state with a fully developed bridging zone, as shown in Fig. 11(d). Once the accumulation of plastic strain reaches the critical threshold of materials, the ligament is damaged as shown in Fig. 11(d). We can clearly observe that extensive plastic deformation has developed within adhesives.

4. The performance of FRP ABJs with different adhesives

Liao et al. (2013) found that the fracture toughness of ABJs changes with the adhesive thickness but demonstrates an opposite trend for different types of adhesive, *i.e.*, ductile and brittle. The mechanical properties of adhesives may also vary the failure behaviors of ABJs subjected to Mode II (da Silva et al., 2010; da Silva and Lopes, 2009). It has been suggested that this difference can be explained by the plasticity of the adhesive layer. In the presence of ligament bridging, adhesive plasticity may contribute more to the overall toughness of joints in terms of ligament elongation. Herein, the model with $\Delta\phi = 0.5\pi$ was employed to investigate the role of the plasticity related properties of adhesives in the failure of ABJs subjected to spatially heterogeneous adhesion.

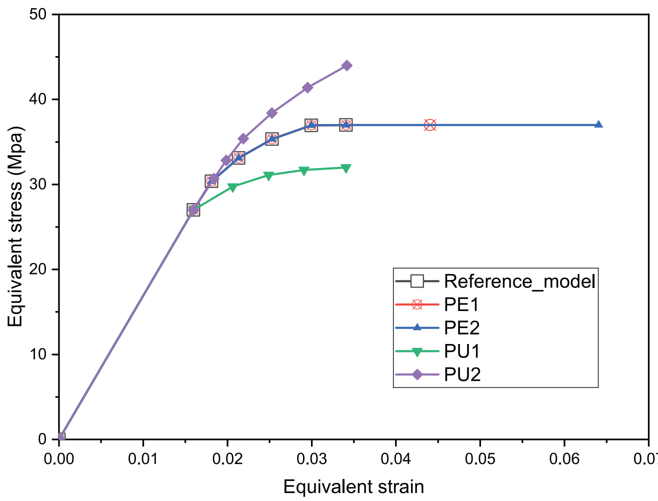

Fig. 12. The applied constitutive models to test the effects of adhesives' properties on the performance of ABJs.

Taking the property parameters presented in Table 2 as a reference, four constitutive models were used to evaluate the effect of adhesives' properties on the crack-tip transfer and ligament bridging, and thus to clarify the associated crack-arrest and toughening mechanisms. The constitutive models of adhesives are as shown in Fig. 12. For PE1 and PE2, we kept the initial yielding strength σ_y and ultimate strength σ_u of adhesives constant to remove the influence of these properties, and we changed the failure strain ϵ_u as 4.4% and 6.4%. For PU1 and PU2, σ_y and ϵ_u were kept constant as listed in Table 2, and σ_u was varied to 32 Mpa and 44 Mpa. The fracture energy for all five constitutive models were kept constant as $G_f = 0.22$ KJ/m^2.

The *R*-curves of the joints with different adhesives are shown in Fig. 13, in which the macroscopic toughness was calculated by integrating the area under the *R*-curve ranging from Δa =15 mm to Δa =24 mm. Fig. 13a confirms that the crack resistance of the joints increased in the presence of ligament bridging when ϵ_u of the adhesives increased. With higher ϵ_u, the ligaments become more stretchable and the bridging length of ligament tend to increase. High elongation and high toughness of the adhesive gave rise to extra debonding surfaces by delaying the fracture of ligaments and more plasticity accumulation within ligaments during large scale bridging. These are the main reasons why the joints show relatively higher macroscopic crack resistance. An increase of ϵ_u from 3.4% to 6.4% resulted in an increase in the effectiveness of crack trapping by about 9.3%. We can reasonably expect that with the increase of ϵ_u, adhesive ligaments can keep their integrity until full debonding of the joint, which may dramatically improve the area of the extra debonding surface and thus the associated dissipation. Based on the above discussions, it will be promising to develop adhesives with high failure strain, ϵ_u, without compromising its adhesion with substrates. Thus, in the presence of proper bonding variability, the crack-arrest features of the system can be developed fully and substantial improvement in ABJs' crack resistance can be achieved. The *R*-curves in Fig. 13b show little difference in the crack resistance for the three joints (nearly overlapped). This indicates that the ultimate strength, σ_u, has less effect and that ligament bridging is not very sensitive to this parameter.

Certainly, all the discussions are conditional depending on a situation where the failure mode of ABJs is dominated by interfacial failure. In the case that the σ_u is smaller than a threshold, pure cohesive failure, rather than interfacial failure, will preferentially happen. In such a scenario, the proposed modeling strategy will encounter challenges of computational convergence.

5. Conclusions and closing remarks

Through modeling the spatial heterogeneity of adhesion with a Gaussian Process, this work improves previously proposed modeling strategies to capture local failure events of secondary bonded composites. We introduced the spatial correlation of adhesion heterogeneity to analyze the effect of spatial heterogeneity and the essential length scales on the bonding toughness enhancement. We varied the correlation length of a Gaussian Process, thereby obtaining joints with continually distributed log-normal G_c and S, with which, the variability of interfacial properties can be characterized in a realistic way, as well as the induced complex debonding mechanisms. Generally, the FRP ABJs can be toughened by the variability of interfacial properties through the participation of extrinsic dissipation during fracture process. Through Monte Carlo simulations, we found that the length scale of spatial correlation has significant effects on the toughening effectiveness. Lower spatial correlation may increase the occurrence of bridging during debonding and the joints demonstrates higher macroscopic toughness.

A joint with periodical fluctuations in adhesion properties was modeled to investigate the effects of the correlation between two

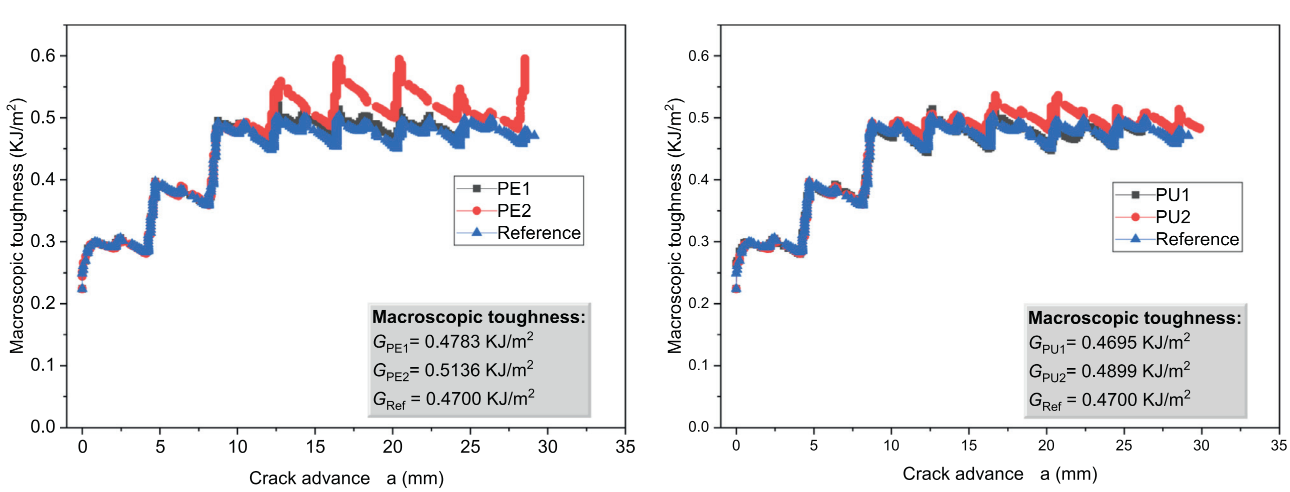

(a) The effect of failure strain (b) The effect of ultimate strength

Fig. 13. The *R*-curves obtained from the joints whose adhesives are with different (a) failure strain ϵ_u and (b) ultimate strength σ_u.

substrates, *i.e.*, the alignment phase $\Delta\phi$ of the adhesion fluctuation between the opposite interfaces. We demonstrated that a minimum phase is needed to periodically trigger the crack-tip transfer and the subsequent bridging, above which there is no significant difference in the effectiveness of crack-arrest. The toughening effect of bridging may be enhanced by increasing the bondline thickness. Nevertheless, the increase of bondline thickness also decreases the qualified range of $\Delta\phi$ to trigger bridging. These insights into the fundamentals of the effects of the correlation in adhesion heterogeneity within each substrate and between two substrates could be applied to improve the design of ABJs with more crack resistance, and improve the design features that enhance material performance.

To identify the importance of the mechanical properties of adhesives, we performed a parametric study. The adhesives' ultimate strengths (over the range of 32 to 44 MPa) were found to have minimal influence on the macroscopic toughness of joints. An increase in ϵ_u from 3.4% to 6.4% resulted in an increase in the effectiveness of crack trapping by about 9.3%. Results from the joints bonded by adhesives with different mechanical properties highlighted the importance of adhesives' ductility in the fracture resistance of ABJs when hybrid failure occurs. These results provide designers with a potential path to exploit the toughening mechanisms by artificially enhancing and controlling the heterogeneity of adhesive bonding, which is expected to produce tougher ABJs without changing the adhesive materials.

Declaration of Competing Interest

The authors declare that they do not have any financial or non-financial conflict of interests

Acknowledgement

The research reported in this publication was supported by funding from King Abdullah University of Science and Technology (KAUST) Office of Sponsored Research (OSR) under award number OSR-2017-CRG6-3388.01.

Appendix A

The mean of the toughness for the two interfaces in the bondline, denoted as G_c^i ($i = 1, 2$) can be regarded as two variables following log-normal distribution, and are independent of each other. The probability density function for G_c^i ($i = 1, 2$) can be expressed as:

$$f\left(G_c^i\right) = \frac{1}{G_c^i\sqrt{2\pi\sigma_{\ln(G_c)}^2}} \exp\left(-\frac{\left(\ln G_c^i - \mu_{\ln(G_c)}\right)^2}{2\sigma_{\ln(G_c)}^2}\right), G_c^i \in (0, +\infty) \tag{A.1}$$

Thus, the joint PDF of (G_c^1, G_c^2) can be expressed as $f(G_c^1)f(G_c^2)$. Provided bridging does not occur during debonding, the crack propagates along the interface with low S and high G_c, two properties which have a negative correlation. Thus the macroscopic toughness of the joint is max(G_c^i), and the expected value of the joint's toughness can be calculated with the following integration:

$$\begin{aligned} G_c^e &= \iint\limits_{G_c^1 \geqslant G_c^2} G_c^1 f\left(G_c^1\right) f\left(G_c^2\right) dG_c^1 dG_c^2 + \iint\limits_{G_c^1 < G_c^2} G_c^2 f\left(G_c^1\right) f\left(G_c^2\right) dG_c^1 dG_c^2 \\ &= \int_0^{+\infty} \left(\int_{G_c^2}^{\infty} G_c^1 f\left(G_c^1\right) dG_c^1\right) f\left(G_c^2\right) dG_c^2 \\ &\quad + \int_0^{+\infty} \left(\int_{G_c^1}^{\infty} G_c^2 f\left(G_c^2\right) dG_c^2\right) f\left(G_c^1\right) dG_c^1 \end{aligned} \tag{A.2}$$

Substituting the characteristic parameters of the stochastic distribution into the above integration, we can theoretically obtain the macroscopic toughness of ABJ with large spatial correlation, which is 0.2624 KJ/m^2, and agrees well with that of the joint subjected to $r = 80$ mm, 0.2598 KJ/m^2, obtained via Monte Carlo simulation.

Appendix B

In general, a non-uniform interface may result in load response exhibiting snap-down (Heide-Jrgensen and Budzik, 2018) or snap-back instability (Xu et al., 2019). Such systems are challenging to analyze under either displacement or force-control using the finite element method since multiple solutions may exist. Here, we presented an analytical solution based on linear elastic fracture mechanics (LEFM) to explain the mismatch between the observed R-curve and the fluctuated input toughness data. The results are discussed within the framework of static analysis.

We applied the corrected beam theory (CBT), accounting for the influence of the end rotation correction (Williams, 1989; Yoshihara

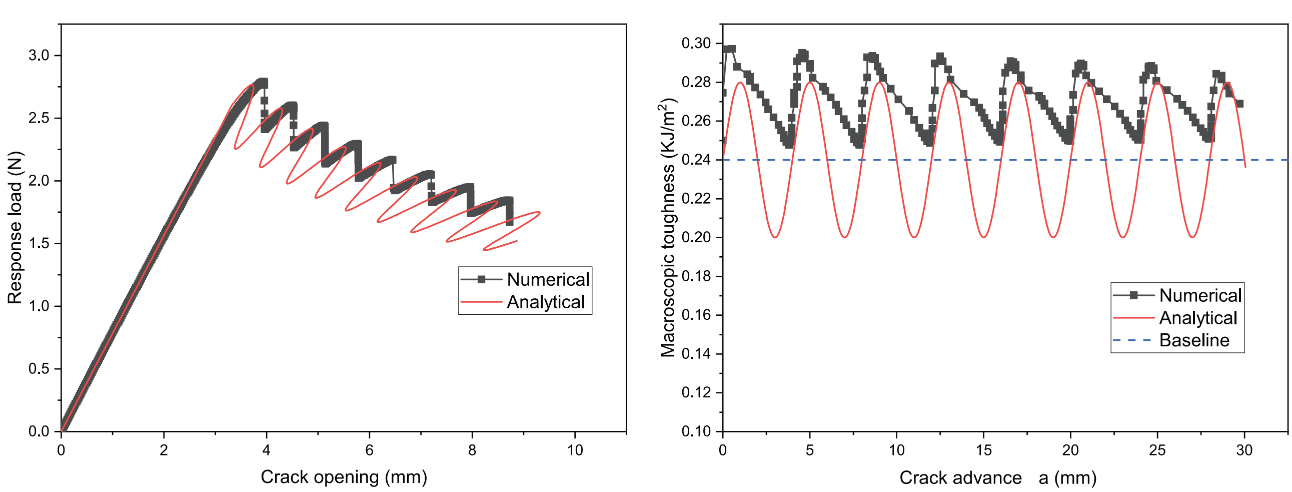

(a) P-δ curves (b) R-curves

Fig. B.14. The $P - \delta$ curves and the R-curves obtained from the joints with fluctuating adhesion.

and Kawamura, 2006) to draw the theoretical solution. According to CBT, the crack opening of DCB specimen is as follows:

$$\delta = \frac{2P(a+\chi h)^3}{3E_{11}I} \tag{B.1}$$

in which P is the applied force, a the crack length, h the height of the cantilever beam, E_{11} the Young's modulus along longitudinal direction and I the second moment of inertial of the DCB arm. χ is the correcting parameter of crack length calculated by:

$$\chi = \left[\frac{1}{13\kappa}\left(\frac{E_{11}}{G_{12}}\right)\left\{3-2\left(\frac{\Gamma}{1+\Gamma}\right)^2\right\}\right]^{1/2} \tag{B.2}$$

where G_{12} is the shear modulus, and κ is the shear stress distribution constant for correcting the deflection caused by the shearing force. Herein, κ is 0.55 determined by fitting the $P-\delta$ curve in the linear regime to the numerical prediction. The coefficient Γ is achieved as follows,

$$\Gamma = \frac{(E_{11}E_{22})^{1/2}}{\kappa G_{12}} \tag{B.3}$$

where E_{22} is Young's modulus in the depth direction. Then applying LEFM, the Mode I energy release rate can be expressed as:

$$G_{cbt}(P,a) = \frac{P^2}{E_{11}Ib}(a+\chi h)^2 \tag{B.4}$$

or

$$G_{cbt}(a,\delta) = \frac{9E_{11}I\delta^2}{4b(a+\chi h)^4} \tag{B.5}$$

Applying Eqs. (B.4) and (B.5), we can obtain the analytical solutions of the $P-\delta$ curve and R-curve as presented in Fig. B.14, which clearly manifest the unstable crack propagation during the DCB test with fluctuating heterogeneity of adhesion. The $P-\delta$ response is found to exhibit snap-back instability at which a positive slope changes to a negative slope, and then snaps back to a certain value where it is actually corresponding to the lowest bound of the input toughness. Afterwards, the crack starts to grow again in a stable manner. Differently, a snap-down response was observed in the numerical simulation, where the applied force dropped onto a smaller value instantaneously after it peaked in one fluctuation, attributed to the incapability of capturing snap-back behavior of iteration algorithms. Thus, the macroscopic toughness shows a mismatch with the analytical R-curve as compared in Fig. B.14b.

Supplementary material

Supplementary material associated with this article can be found, in the online version, at 10.1016/j.ijsolstr.2020.04.012.

References

Ahrendt, P., 2005. The Multivariate Gaussian Probability Distribution. Tech. Rep.. Technical University of Denmark.

Akisanya, A.R., 2006. An alternating crack growth in adhesively bonded joints. In: Fracture of Nano and Engineering Materials and Structures. Springer, pp. 915–916.

Akisanya, A.R., Fleck, N.A., 1992. Brittle fracture of adhesive joints. Int. J. Fract. 58 (2), 93–114.

Ashcroft, I.A., Khokar, Z.R., Silberschmidt, V.V., 2012. Modelling the effect of microstructural randomness on the mechanical response of composite laminates through the application of stochastic cohesive zone elements. Comput. Mater. Sci 52 (1), 95–100.

Belnoue, J.P.H., Hallett, S.R., 2016. Cohesive/adhesive failure interaction in ductile adhesive joints part i: a smeared-crack model for cohesive failure. Int. J. Adhes. Adhes. 68, 359–368.

Berry, J., 1963. Determination of fracture surface energies by the cleavage technique. J. Appl. Phys. 34 (1), 62–68.

Bower, A.F., Ortiz, M., 1991. A three-dimensional analysis of crack trapping and bridging by tough particles. J. Mech. Phys. Solids 39 (6), 815–858.

Budhe, S., Banea, M.D., de Barros, S., da Silva, L.F.M., 2017. An updated review of adhesively bonded joints in composite materials. Int. J. Adhes. Adhes. 72, 30–42.

Campilho, R.D.S.G., Banea, M.D., Pinto, A.M.G., da Silva, L.F.M., de Jesus, A.M.P., 2011. Strength prediction of single- and double-lap joints by standard and extended finite element modelling. Int. J. Adhes. Adhes. 31 (5), 363–372.

Canal, L.P., Alfano, M., Botsis, J., 2017. A multi-scale based cohesive zone model for the analysis of thickness scaling effect in fiber bridging. Compos. Sci. Technol. 139, 90–98.

Canal, L.P., Pappas, G., Botsis, J., 2016. Large scale fiber bridging in mode I intralaminar fracture. an embedded cell approach. Compos. Sci. Technol. 126, 52–59.

Cao, H.C., Evans, A.G., 1989. An experimental study of the fracture resistance of bimaterial interfaces. Mech. Mater. 7 (4), 295–304.

Chopin, J., Boudaoud, A., Adda-Bedia, M., 2015. Morphology and dynamics of a crack front propagating in a model disordered material. J. Mech. Phys. Solids 74, 38–48.

Cooper, V., Ivankovic, A., Karac, A., McAuliffe, D., Murphy, N., 2012. Effects of bond gap thickness on the fracture of nano-toughened epoxy adhesive joints. Polymer 53 (24), 5540–5553.

Da Silva, L.F., Campilho, R.D., 2012. Advances in numerical modelling of adhesive joints. In: Advances in Numerical Modeling of Adhesive Joints. Springer, pp. 1–93.

Dalmas, D., Barthel, E., Vandembroucq, D., 2009. Crack front pinning by design in planar heterogeneous interfaces. J. Mech. Phys. Solids 57 (3), 446–457.

De Moura, M., Daniaud, R., Magalhaes, A., 2006. Simulation of mechanical behaviour of composite bonded joints containing strip defects. Int. J. Adhes. Adhes. 26 (6), 464–473.

Dimas, L.S., Giesa, T., Buehler, M.J., 2014. Coupled continuum and discrete analysis of random heterogeneous materials: elasticity and fracture. J. Mech. Phys. Solids 63, 481–490.

Dimas, L.S., Veneziano, D., Buehler, M.J., 2016. Strength and fracture toughness of heterogeneous blocks with joint lognormal modulus and failure strain. J. Mech. Phys. Solids 92, 72–86.

Dimas, L.S., Veneziano, D., Giesa, T., Buehler, M.J., 2015. Probability distribution of fracture elongation, strength and toughness of notched rectangular blocks with lognormal young's modulus. J. Mech. Phys. Solids 84, 116–129.

Haider, A.-Z., Zhao, X.-L., Al-Mihaidi, R., 2011. Mechanical behaviour of normal modulus carbon fibre reinforced polymer (CFRP) and epoxy under impact tensile loads. Procedia Eng. 10, 2453–2458.

Heide-Jrgensen, S., Budzik, M.K., 2018. Effects of bondline discontinuity during growth of interface cracks including stability and kinetic considerations. J. Mech. Phys. Solids 117, 1–21.

Hillerborg, A., Modéer, M., Petersson, P.-E., 1976. Analysis of crack formation and crack growth in concrete by means of fracture mechanics and finite elements. Cem. Concr. Res. 6 (6), 773–781.

Kammer, D.S., Munoz, D.P., Molinari, J.F., 2016. Length scale of interface heterogeneities selects propagation mechanism of frictional slip fronts. J. Mech. Phys. Solids 88, 23–34.

Kaute, D.A.W., Shercliff, H.R., Ashby, M.F., 1993. Delamination, fibre bridging and toughness of ceramic matrix composites. Acta Metall. Mater. 41 (7), 1959–1970.

Khokhar, Z.R., Ashcroft, I.A., Silberschmidt, V.V., 2009. Simulations of delamination in CFRP laminates: effect of microstructural randomness. Comput. Mater. Sci. 46 (3), 607–613.

Kim, J., Kim, D.W., Baik, S., Hwang, G.W., Kim, T.-i., Pang, C., 2019. Snail-inspired dry adhesive with embedded microstructures for enhancement of energy dissipation. Adv. Mater. Technol. 1900316.

Li, X., Tao, R., Alfano, M., Lubineau, G., 2020. How variability in interfacial properties results in tougher bonded composite joints by triggering bridging. Int. J. Solids Struct. 191–192, 87–98.

Liao, L., Huang, C., Sawa, T., 2013. Effect of adhesive thickness, adhesive type and scarf angle on the mechanical properties of scarf adhesive joints. Int. J. Solids Struct. 50 (25–26), 4333–4340.

Liner, M., Alabort, E., Cui, H., Rito, R., Blackman, B.R.K., Petrinic, N., 2019. Experimental characterisation and numerical modelling of the influence of bondline thickness, loading rate, and deformation mode on the response of ductile adhesive interfaces. J. Mech. Phys. Solids 130, 349–369.

lvarez, D., Blackman, B.R.K., Guild, F.J., Kinloch, A.J., 2014. Mode I fracture in adhesively-bonded joints: amesh-size independent modelling approach using cohesive elements. Eng. Fract. Mech. 115, 73–95.

Meng, F., Thouless, M.D., 2019. Cohesive-zone analyses with stochastic effects, illustrated by an example of kinetic crack growth. J. Mech. Phys. Solids 132, 103686.

Mohamed, G., Allegri, G., Yasaee, M., Hallett, S.R., 2018. Cohesive element formulation for z-pin delamination bridging in fibre reinforced laminates. Int. J. Solids Struct. 132–133, 232–244.

Moroni, F., Musiari, F., Romoli, L., Pirondi, A., 2018. Influence of laser treatment parameters on the mode i strain energy release rate of aluminum double cantilever beam joints. Int. J. Adhes. Adhes. 83, 31–40.

Motamedi, D., Milani, A.S., Komeili, M., Bureau, M.N., Thibault, F., Trudel-Boucher, D., 2014. A stochastic XFEM model to study delamination in PPS/Glass UD composites: effect of uncertain fracture properties. Appl. Compos. Mater. 21 (2), 341–358.

Mower, T.M., Argon, A.S., 1995. Experimental investigations of crack trapping in brittle heterogeneous solids. Mech. Mater. 19 (4), 343–364.

Naya, F., Pappas, G., Botsis, J., 2019. Micromechanical study on the origin of fiber bridging under interlaminar and intralaminar mode I failure. Compos. Struct. 210, 877–891.
Pappas, G.A., Botsis, J., 2020. Variations on R-curves and traction-separation relations in DCB specimens loaded under end opening forces or pure moments. Int. J. Solids Struct. 191–192, 42–55.
Saldanha, D.F.S., Canto, C., da Silva, L.F.M., Carbas, R.J.C., Chaves, F.J.P., Nomura, K., Ueda, T., 2013. Mechanical characterization of a high elongation and high toughness epoxy adhesive. Int. J. Adhes. Adhes. 47, 91–98.
Sills, R.B., Thouless, M.D., 2015. Cohesive-length scales for damage and toughening mechanisms. Int. J. Solids Struct. 55, 32–43.
da Silva, L.F.M., Lopes, M.J.C.Q., 2009. Joint strength optimization by the mixed-adhesive technique. Int. J. Adhes. Adhes. 29 (5), 509–514.
da Silva, L.F.M., de Magalhes, F.A.C.R.G., Chaves, F.J.P., de Moura, M.F.S.F., 2010. Mode II fracture toughness of a brittle and a ductile adhesive as a function of the adhesive thickness. J. Adhes. 86 (9), 891–905.
Sørensen, B.F., Jacobsen, T.K., 1998. Large-scale bridging in composites: R-curves and bridging laws. Composites Part A 29 (11), 1443–1451.
de Souza Neto, E.A., Peric, D., Owen, D.R., 2011. Computational Methods for Plasticity: Theory and Applications. John Wiley & Sons.
Sun, D.-x., Yang, C.-j., Qi, X.-d., Yang, J.-h., Wang, Y., 2018. Largely enhanced fracture toughness of the PP/EPDM blends induced by adding carbon nanofibers. Compos. Sci. Technol. 164, 146–152.
Srensen, B.F., Jacobsen, T.K., 1998. Large-scale bridging in composites: R-curves and bridging laws. Compos. Part A 29 (11), 1443–1451.
Taleb Ali, M., Jumel, J., Shanahan, M.E.R., 2018. Effect of adhesion defects on crack propagation in double cantilever beam test. Int. J. Adhes. Adhes. 84, 420–430.
Tan, G., Zhang, J., Zheng, L., Jiao, D., Liu, Z., Zhang, Z., Ritchie, R.O., 2019. Nature-inspired nacre-like composites combining human tooth-matching elasticity and hardness with exceptional damage tolerance. Adv. Mater. 31 (52), e1904603.
Tao, R., Alfano, M., Lubineau, G., 2018. Laser-based surface patterning of composite plates for improved secondary adhesive bonding. Composites Part A 109, 84–94.
Tao, R., Alfano, M., Lubineau, G., 2019. In-situ analysis of interfacial damage in adhesively bonded composite joints subjected to various surface pretreatments. Composites Part A 116, 216–223.
Tenchev, R.T., Falzon, B.G., 2007. Experimental and numerical study of debonding in composite adhesive joints. In: 16th International Conference on Composite Materials, Kyoto, Japan.
Williams, J.G., 1989. End corrections for orthotropic DCB specimens. Compos. Sci. Technol. 35 (4), 367–376.
Xu, W., Yu, H.C., Tao, C.H., 2014. Influence of randomly distributed adhesive properties on the overall mechanical response of metallic adhesively bonded joints. Int. J. Adhes. Adhes. 52, 48–56.
Xu, Y., Singh, Y., Pan, C., Subbarayan, G., 2019. Adhesive toughness and instability in bonded heterogeneous films. Int. J. Solids Struct. 169, 41–54.
Yang, C., Huang, H., Tomblin, J.S., Sun, W., 2004. Elastic-plastic model of adhesive-bonded single-lap composite joints. J. Compos. Mater. 38 (4), 293–309.
Yoshihara, H., Kawamura, T., 2006. Mode I fracture toughness estimation of wood by DCB test. Composites Part A 37 (11), 2105–2113.